# Solvothermal Preparation of an Electrocatalytic Metalloporphyrin MOF Thin Film and its Redox Hopping Charge-Transfer Mechanism

Spencer R. Ahrenholtz, Charity C. Epley, and Amanda J. Morris*

Department of Chemistry, Virginia Tech, Blacksburg, Virginia 24061, United States

ⓢ Supporting Information

**ABSTRACT:** A thin film of a metalloporphyrin metal−organic framework consisting of [5,10,15,20-(4-carboxyphenyl)porphyrin]Co(III) (CoTCPP) struts bound by linear trinuclear $Co^{II}$-carboxylate clusters has been prepared solvothermally on conductive fluorine-doped tin oxide substrates. Characterization of this mesoporous thin film material, designated as CoPIZA/FTO, which is equipped with large cavities and access to metal active sites, reveals an electrochemically active material. Cyclic voltammetry displays a reversible peak with $E_{1/2}$ at −1.04 V vs ferrocyanide attributed to the ($Co^{III/II}$TCPP)CoPIZA redox couple and a quasi-reversible peak at −1.45 V vs ferrocyanide, which corresponds to the reduction of ($Co^{II/I}$TCPP)CoPIZA. Analysis of the spectroelectrochemical response for the ($Co^{II/I}$TCPP)CoPIZA redox couple revealed non-Nernstian reduction with a nonideality factor of 2 and an $E_{1/2}$ of −1.39 V vs ferrocyanide. The film was shown to retain its structural integrity with applied potential, as was demonstrated spectroelectrochemically with maintenance of isosbestic points at 430, 458, and 544 nm corresponding to the ($Co^{III/II}$TCPP)CoPIZA transition and at 390 and 449 nm corresponding to the ($Co^{II/I}$TCPP)CoPIZA transition. The mechanism of charge transport through the film is proposed to be a redox hopping mechanism, which is supported by both cyclic voltammetry and spectroelectrochemistry. A fit of the time-dependent spectroelectrochemical data to a modified Cottrell equation gave an apparent diffusion coefficient of 7.55 ($\pm$0.05) $\times$ $10^{-14}$ $cm^2$/s for ambipolar electron and cation transport throughout the film. Upon reduction of the metalloporphyrin struts to ($Co^{I}$TCPP)CoPIZA, the CoPIZA thin film demonstrated catalytic activity for the reduction of carbon tetrachloride.
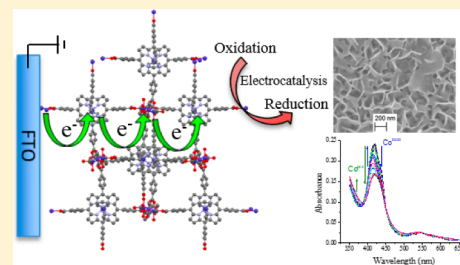
## INTRODUCTION

Metal−organic frameworks (MOFs) are 3D porous crystalline networks formed through the orientation of metal nodes by multidentate organic linkers.[1,2] The porous nature of these materials has led to various applications in gas storage and separation as well as drug delivery.[3−7] High surface area, porous materials also have tremendous potential for use in catalysis.[8,9] Theoretically, every catalytic center in the MOF (metal or linker) is accessible for reactivity. Therefore, less material is required in comparison to traditional approaches. Indeed, MOFs have proven to be excellent scaffolds for Lewis acid catalyzed reactions as well as enantioselective catalysis.[9,10]

Critical environmentally relevant catalytic processes including $CO_2$ reduction, $H_2O$ oxidation, and $H^+$ reduction rely on electron-transfer reactivity. Therefore, MOFs capable of driving electron-transfer chemistry have the potential to revolutionize the field of envirocatalysis. However, the intrinsic insulating nature of the caboxylate bonds utilized to form MOFs results in low conductivity.[11] Some focus has been placed on the use of band structure to explain electron transport through MOFs.[12−14] However, the predicted band gaps are well above kT and cannot explain conduction in the dark. Also, MOFs are "soft" materials that, upon the addition of charge, are likely to reorganize locally, causing disruption to the band structure. Therefore, the nature of electron transfer through MOFs is most likely an electron hopping mechanism, similar to that demonstrated by Murray in Os and Fe polypyridine redox polymers.[15]

There have been various investigations into photoinitiated electron transfer through MOFs. Indeed, MOFs containing known photoactive $H_2O$ oxidation and $CO_2$ reduction catalysts have been shown to reduce their substrates with moderate efficiency.[16] In these studies, photoinitiated electron migration to the surface of MOF particles was faster than catalysis. Therefore, while these materials are insulating, conductivity is not limiting. That being said, the conductivity of MOFs has been synthetically tuned by building in linear molecular chains poised for redox hopping throughout the framework.[17,18] In light of this elegant work on photoelectron transfer, few studies on electrochemically driven catalysis exist in the literature.[19−21] Of those that do appear, it is unclear whether the observed reactivity occurs at electrodeposited metals or metal oxides formed at highly reducing or oxidizing potentials or the MOF itself.[22,23]

Metalloporphyrins (Fe and Co) have been shown to promote the reduction of various substrates including $H^+$, $CO_2$, and organohalides.[24−27] In addition, their spectral properties (large extinction coefficients and distinct spectra sensitive to varying oxidation state)[28] make them ideal

candidates for spectroelectrochemical studies. Various porous materials comprised of porphyrins have been developed,[29] including porphyrinic MOFs with open accessibility to redox active metal centers.[30−36] Efficient exciton migration through a zinc-metalated porphyrin MOF developed by Hupp et al. has been observed.[37]

For electrocatalysis, it is advantageous to prepare the MOF as a thin film, allowing for direct attachment to the electrode surface, control of film thickness, and unobstructed access to pore cavities and available active sites.[38,39] To date, there exist several methods for the preparation of MOF thin films onto substrates.[38,39] These include the direct adsorption of densely packed individual crystallites formed or preformed in solution onto a modified or unmodified surface and a layer-by-layer (LBL) approach, in which the substrate is alternately exposed to solutions containing metal and linker(s) yielding films of uniform crystallinity whose growth is directional.[40−44] Recently, a LBL approach for oriented porphyrin films has been developed.[44] Porphyrin MOF thin films have previously been prepared by a Langmuir−Blodgett approach yielding layered 2D films.[45−47] Porphyrinic thin films grown directly onto a substrate surface via an alternative third approach, termed solvothermal deposition, have not yet been reported.

Herein, we report the first solvothermal synthesis and spectroelectrochemical investigation of a redox active porphyrinic-MOF thin film for application in envirocatalysis. The metalloporphyrin MOF contains [5,10,15,20-(4-carboxyphenyl) porphyrin]Co(III) (CoTCPP) struts bound by linear trinuclear $Co^{II}$-carboxylate clusters to form a porous network with large channels (Figure 1).[31] The film, grown on a
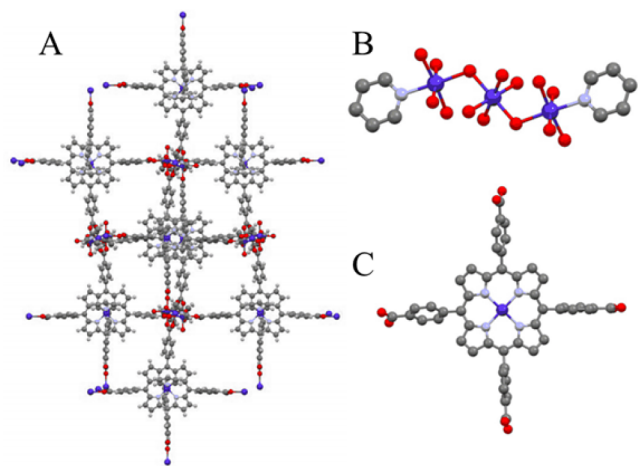


**Figure 1.** (A) CoPIZA as viewed down the (100) direction showing the large channels in the MOF network. (B) Cobalt clusters of CoPIZA; (C) CoTCPP within the CoPIZA framework.[31]

conductive fluorine-doped tin oxide (FTO) substrate, is designated as CoPIZA/FTO and displayed a reversible electrochemical response while maintaining structural integrity. This provided a scaffold for detailed mechanistic investigation into the action of charge transfer through MOF materials. Analysis of the electrochemical response supports a redox hopping mechanism for charge transport. Lastly, the intact MOF film was demonstrated to be catalytically active, promoting $CCl_4$ reduction.

## ■ RESULTS AND DISCUSSION

**Synthesis and Structural Characterization.** CoPIZA/FTO was prepared solvothermally via templation by a self-assembled monolayer (SAM) of the porphyrin linker adsorbed onto the FTO substrate. The SAM was formed by immersion of the FTO in a solution of tetrakis(4-carboxyphenyl)porphyrin (TCPP) overnight. X-ray photoelectron spectroscopy (XPS) confirmed SAM formation. The observed N1s peak at 401 eV is attributed to the pyrrole nitrogens of the TCPP (Figure 2A).[48]
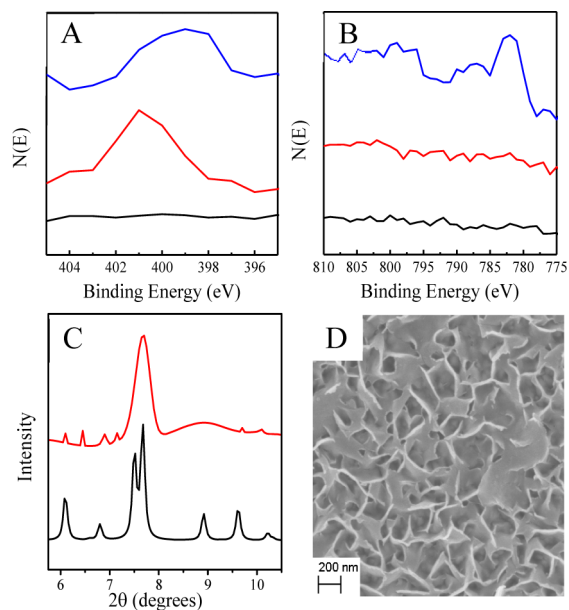


**Figure 2.** XPS of FTO (black), the TCPP SAM/FTO (red), and CoPIZA/FTO (blue) showing the N1s peak (A) and Co2p peak (B). (C) PXRD pattern of CoPIZA/FTO (red) and the simulated CoPIZA single crystal pattern (black). (D) SEM image of CoPIZA/FTO.

The SAM-coated FTO was then transferred to a glass tube, followed by the addition of $Co(II)Cl_2 \cdot 6H_2O$, TCPP, and an aqueous pyridine/KOH solution.[31] Under solvothermal conditions, the metalloporphyrin MOF grew directly onto the FTO substrate, confirmed by XPS, powder X-ray diffraction (PXRD), and scanning electron microscopy (SEM) (Figure 2). XPS confirmed CoPIZA formation after the solvothermal reaction, as indicated by peaks at 782 and 798 eV corresponding to the Co2p binding energy (Figure 2B, blue). The N1s peak of CoPIZA (Figure 2A, blue) is broadened, consistent with both the pyrrole nitrogens of TCPP and the addition of bound pyridine in the cobalt clusters of the MOF network.[48]

The PXRD of the CoPIZA/FTO displays peaks at 6.1, 6.9, 7.6, 9.7, and 10.1° (Figure 2C, red) that coincide with those of the simulated CoPIZA pattern based on the single crystal data previously reported (Figure 2C, black).[31] There are peaks present at 6.4 and 7.2° in the CoPIZA/FTO pattern that are absent from the CoPIZA single crystal pattern, which, as a result of the orientation and layering of the MOF crystallites in the film, can be due to the multiple diffractions of the X-ray beam from the individual crystallites or unknown impurities.[49] The full PXRD pattern (Figure S1) displays intense peaks at larger angles that can be attributed to the FTO substrate. The SEM image of the CoPIZA film (Figure 2D) shows a crystalline network on the surface. The height and topography of the

2465

dx.doi.org/10.1021/ja410684q | J. Am. Chem. Soc. 2014, 136, 2464−2472

network was investigated using atomic force microscopy (AFM) imaging. The network was found to range between 80 and 500 nm in thickness (Figure S2).

Fourier-transform infrared (FTIR) spectroscopy was used to characterize CoPIZA/FTO, TCPP, and metalated CoTCPP (Figure 3A). The TCPP and CoTCPP spectra (black and red,
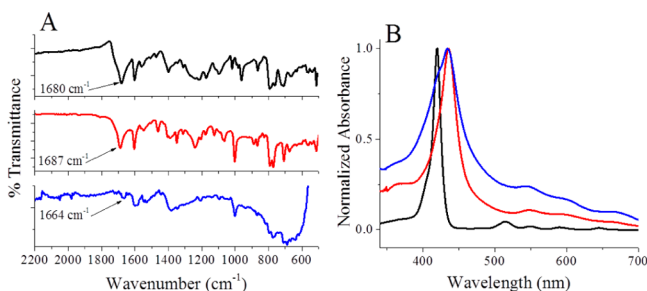


**Figure 3.** (A) ATR-FTIR spectra of TCPP (black), CoTCPP (red), and CoPIZA/FTO (blue). (B) Normalized UV−vis spectra of TCPP/DMF (black), CoPIZA/FTO/DMF (red), and CoPIZA/FTO/DMF after purging with nitrogen (blue).

respectively) show features corresponding to the C═O stretch of the carboxylic acids at 1680 and 1687 cm$^{-1}$, respectively, and a peak at 1600 cm$^{-1}$, which corresponds to the C═C stretch of the aromatic carbons of the macrocycle. The CoPIZA/FTO spectrum (blue) shows a shift of the carboxylate stretching band to lower frequency at 1664 cm$^{-1}$, due to the transformation of the carboxylic acid groups of the free porphyrin to the carboxylato chelating functionality in the MOF.

The steady-state absorption spectrum of TCPP in DMF was characteristic of free-base porphyrins of $D_{2h}$ symmetry in solution, displaying an intense Soret band in the near UV region centered at 420 nm and four low energy Q bands in the visible region occurring at 515, 549, 590, and 645 nm (Figure 3B, black).[50] Upon chelation to the porphyrinic nitrogens to the Co$^{III}$ metal center in CoPIZA/FTO, the symmetry increases to $D_{4h}$ and is accompanied by a red shift of the Soret band to 436 nm and collapse of the four Q-bands into two bands at 548 and 595 nm (Figure 3B, red). After purging with nitrogen, CoPIZA/FTO/DMF displayed spectral characteristics of both Co$^{III}$TCPP and Co$^{II}$TCPP, as Co$^{III}$TCPP/CoPIZA undergoes autoreduction by electron donating axial pyridine ligands to form Co$^{II}$TCPP/CoPIZA (Figure 3B, blue).[51] The Co-carboxylate clusters in the CoPIZA framework are also expected to absorb light but are not observed in the steady-state absorption spectra due to the large extinction coefficient of CoTCPP ($\sim$10$^5$ M$^{-1}$ cm$^{-1}$).[27] The effect of varying the pyridine concentration in the solvothermal film synthesis was also investigated using UV−vis spectroscopy. It was observed that with increasing pyridine concentration, the absorbance decreased while the peak wavelength exhibited a red shift (Figure 4). This is attributed to pyridine's effect on the equilibrium between solid CoPIZA crystallites and the molecular components in solution as well as the CoTCPP ligation environment.

**Investigation of Charge-Transfer Mechanism.** With CoPIZA/FTO in hand, efforts shifted to characterizing the charge-transport properties of the material. There has been some effort in the literature to computationally determine the energetic position of the filled and unfilled states in MOFs.[8,12,13] In doing so, some have characterized MOFs as
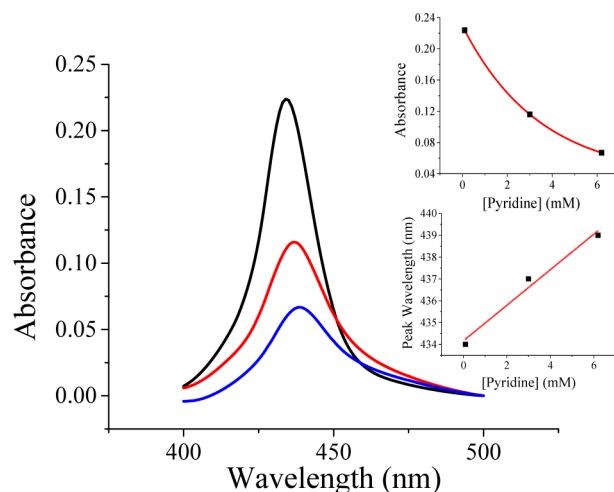


**Figure 4.** Steady-state UV−vis absorption spectra of CoPIZA/FTO synthesized with varying pyridine concentration. With increasing pyridine concentration, the absorbance of the Soret band decreased (inset top), while the Soret band wavelength displayed a red shift (inset bottom).

"semiconductors", with valence and conduction bands comprised of overlapping molecular HOMO and LUMO orbitals.[52,53] CoPIZA is constructed by CoTCPP struts and trimeric cobalt clusters (Figure 1).[31] The bonds forming the cobalt clusters are carboxylate in nature. Carboxylate bonds are known to be insulating and, therefore, it is unlikely that sufficient HOMO−LUMO overlap exists between the two molecular components to justify a band structure. Hence, CoPIZA is proposed to be a 3D network of individual redox centers.

Keeping this in mind, the conductivity of the CoPIZA is expected to be moderate on the edge of insulating. This is indeed the case, as was explored by electrochemical impedance spectroscopy (Figure S3). The measured conductivity, determined by the reciprocal of the area and thickness corrected low frequency intercept of the Nyquist plot, was $3.62 \times 10^{-8}$ S cm$^{-1}$ and places the film's dark conductivity on the order of wide band gap semiconductors, $\sigma_{TiO_2} = 1 \times 10^{-11}$ S cm$^{-1}$,[54] and common organic semiconductors, $\sigma_{polybithiophene} = 1 \times 10^{-8}$.[55,56] Therefore, CoPIZA/FTO is semiconducting but not necessarily a semiconductor. It is important to note that moderate conductivity does not preclude charge-transfer chemistry upon applied potential. In fact, there are a number of examples of electrocatalysis at the surface of TiO$_2$.[57−60]

Given the almost insulating behavior of CoPIZA/FTO, charge transfer is likely to occur via a redox hopping mechanism.[14] Vital to such a mechanism is the need for the redox centers to have similar or the same reduction potentials and individual immobilized units to be close enough for efficient hopping. Otherwise, an entire molecular component can act as an insulating block to electronic communication across the material. Cyclic voltammetric (CV) analysis of CoPIZA/FTO in 0.1 M LiClO$_4$/DMF displays two cathodic peaks at −1.1 and −1.45 V and, upon the reverse scan, one anodic peak at −0.975 V vs ferrocyanide (Figure 5). Voltammograms collected over a smaller potential window (−0.4 to −1.2 V) indicate that the first cathodic wave and the anodic wave correspond to a coupled, reversible redox event (Figure S4). The cathodic and anodic peak currents ($i_{pc}$ and $i_{pa}$, respectively) were equal at $\sim$2.9 μA. The observed peak
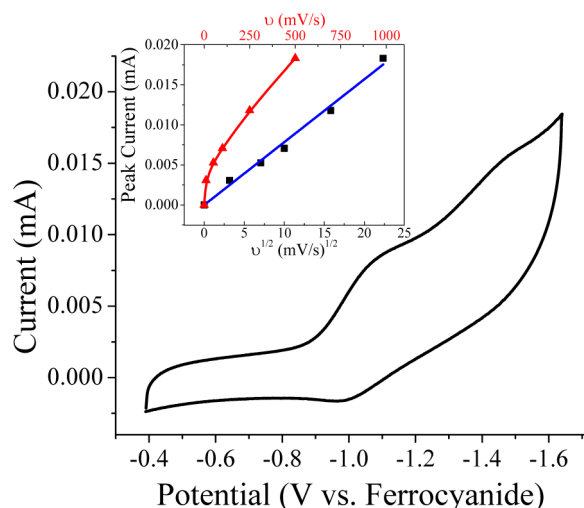
**Figure 5.** Cyclic voltammetry of the CoPIZA/FTO in 0.1 M LiClO$_4$/DMF at 100 mV/s. Inset shows the peak current of the reduction at −1.1 V vs ferrocyanide to be linear with the square root of the scan rate $(\upsilon)^{1/2}$.

separation $(\Delta E_p)$ was 125 mV. Theoretically, a reversible process should have a peak separation of 59 mV/$n$, where $n$ is the number of electrons transferred. However, peak separation of that magnitude is rarely observed in laboratory experiments, due to uncompensated ohmic drops in the electrochemical setup (*vide infra*). Therefore, experimental convention defines reversibility at a boundary of approximately 120 mV/$n$ . Based on this modified criterion, the first electrochemical wave is reversible.

For a redox hopping mechanism to explain the observed electrochemical events, the response must obey Fick's law of diffusion. This can result in electrochemical signatures unexpected for materials with fixed redox centers, like that in CoPIZA/FTO. The electrochemical response observed in CV is dependent upon the diffusion coefficient ($D$), and, thus, the rate of charge transport ($k_{ct}$).[61] There are three regimes to observed rate-dependent electrochemical responses: (i) $k_{ct} >$ scan rate ($\upsilon$), (ii) $k_{ct} \approx \upsilon$, and (iii) $k_{ct} < \upsilon$.[61−63]

In the first regime (rapid charge transport), the CV will display electrochemical peaks that have a symmetric shape ($\Delta E_p = 0$) centered about the reduction potential. Additionally, the observed peak current should be proportional to the scan rate. This is exemplified in the work of Chidsey on ferrocene-terminated, thiol-based SAM-modified gold electrodes.[64] In this classic example, the anodic and cathodic peaks occurred at the same potential with the theoretically predicted ideal 90 mV peak width at half of the maximum current. In addition to this work, a similar response has been observed with various surface immobilized systems.[62,65−68]

CoPIZA/FTO exhibits nonzero, scan-rate dependent $\Delta E_p$ at all scan rates applied (10−1000 mV/s). Such behavior is most consistent with regime (iii). In this regime, the CV behavior is quantitatively the same as freely diffusing redox centers in solution. Therefore, the current response should obey the Randles−Sevcik equation, eq 1:

$$i_p = 0.4463 nFAC \left( \frac{nF\upsilon D}{RT} \right)^{1/2} \quad (1)$$

where $i_p$ is the peak current, $n$ is the number of electrons transferred, $F$ is Faraday's constant, $A$ is the electrode area, $C$ is

the concentration of redox active species, $\upsilon$ is scan rate, $D$ is the diffusion coefficient, $R$ is the gas constant, and $T$ is temperature. Thus, the peak current should be linear with a function of $\upsilon^{1/2}$.

The inset in Figure 5 shows the relationship between $i_{pc}$ at −1.1 V vs a function of $\upsilon$. As mentioned above, for diffusion-limited processes like those in regime (iii), a linear relationship between $i_{pc}$ and $\upsilon^{1/2}$ is expected via Randles−Sevcik.[61,69] Mass-transfer independent redox reactions, like those observed in the rapid charge-transfer limit, are expected to exhibit a linear relationship between current and $\upsilon$.[61,62] Plots of both $i_{pc}$ vs $\upsilon^{1/2}$ (diffusion limited) and $i_{pc}$ vs $\upsilon$ (mass transfer independent) resulted in statistically linear relationships, $R^2 = 0.99$ and 0.97, respectively. However, there is a pronounced curvature visible in the $i_{pc}$ vs $\upsilon$ relation, and thus, the results are consistent with a diffusion-limited ($k_{ct} < \upsilon$) redox reaction that occurs via redox hopping charge transport.

The first to propose a redox hopping mechanism for charge transport were Kauffmann and Engler for polymers with incorporated redox-active pyrazoline units.[70−72] It has since been expanded to polymeric systems containing immobilized inorganic compounds (ferrocene and ruthenium trisbipyridine).[62,64−68,73] Qualitatively and quantitatively the results presented here agree with these prior investigations. More recently, Scholz predicted, through a theoretical treatment, that similar electrochemical responses would be observed for immobilized microcrystals, similar to MOFs.[22,74−76] Although Scholz's exact theoretical framework cannot be applied to the experimental data collected for CoPIZA/FTO due to the inhomogeneity of crystal packing, shape, and size, the results represent the first quantitative support for his model.

In CoPIZA/FTO there are two components that could be the source of the observed electrochemical response, CoTCPP, and the trimeric cobalt clusters. Cyclic voltammetry only provides the potential required to transport electrons and does not identify the active species. Therefore, spectroelectrochemical measurements were utilized to determine the molecular origin of the observed electrochemical peaks. An electrochemical cell was constructed in a N$_2$-purged quartz cuvette and placed in a UV−vis spectrometer. The spectral changes were then monitored as a function of applied potential. At an applied potential of −1000 mV vs ferrocyanide, there was an observed decrease in the Soret band of (Co$^{III}$TCPP)CoPIZA at 436 nm accompanied by an increase in the Soret band of (Co$^{II}$TCPP)CoPIZA at 419 nm with maintenance of isosbestic points at 430, 458, and 544 nm (Figure 6 top inset, red; Figure S5). Thus, the reduction peak observed at −1.04 V is due to (Co$^{III/II}$TCPP)CoPIZA reduction. With increasing negative potential, the Soret band of (Co$^{II}$TCPP)CoPIZA was found to decrease in intensity with the appearance of a split Soret (419 and 430 nm) and an increase in absorbance at 370 nm, attributed to (Co$^{I}$TCPP)CoPIZA. The (Co$^{II/I}$TCPP)CoPIZA redox transition is also accompanied by isosbestic points at 390 and 449 nm (Figure S6).

The Nernst equation (eq 2) states that when a redox couple is 50% reduced and 50% oxidized, the applied potential is equal to the $E_{1/2}$ (the standard reduction potential at nonunit molarity). Since the spectroelectrochemical data provide a direct measure of the ratio of reduced/oxidized species in the absence of other electrochemical events, a rearrangement of the Nernst equation to solve for the percent reduced species ($x$) (eq 3) allows for the determination of $E_{1/2}$ for the Co$^{II}$/Co$^{I}$TCPP redox couple. However, the spectral data could not
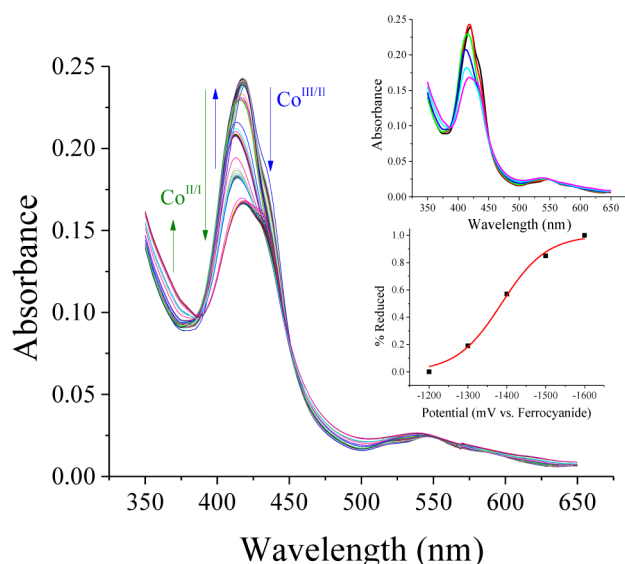
**Figure 6.** Absorption spectra recorded for CoPIZA/FTO as the applied potential was changed. Top inset shows the absorption spectra of CoPIZA/FTO (black) and with applied potentials (vs ferrocyanide) of −1000 mV (red), −1300 mV (green), −1400 mV (blue), −1500 mV (cyan), and −1600 mV (magenta). Bottom inset displays the sigmoidal fit of the percent of reduced cobalt present at the applied potential (eq 5).

be adequately fit to eq 3, suggesting the process deviates from Nernstian behavior.

$$E = E_{1/2} - \frac{59\text{mV}}{n}\log_{10}\left(\frac{[\text{red}]}{[\text{ox}]}\right) \qquad (2)$$

$$x = \frac{1}{1 + 10^{(E_{\text{app}} - E_{1/2})/59}} \qquad (3)$$

A modification of the Nernst equation with the inclusion of a nonideality factor ($a$), a measure of deviation from Nernstian behavior, (eq 4), and rearrangement to solve for $x$ (eq 5) allowed for an accurate fit of the spectral data. The nonideality factor obtained was 2. Thus, for an order of magnitude change in [reduced CoPIZA]/[oxidized CoPIZA], 118 mV needs to be applied to the film.

$$E = E_{1/2} - \frac{59\text{mV}*a}{n}\log_{10}\left(\frac{[\text{red}]}{[\text{ox}]}\right) \qquad (4)$$

$$x = \frac{1}{1 + 10^{(E_{\text{app}} - E_{1/2})/59a}} \qquad (5)$$

Additionally, the $E_{1/2}$ for the (Co$^{II/I}$TCPP)CoPIZA transition was determined via eq 5 to be −1386 ± 6 mV vs ferrocyanide. This is consistent with the second redox feature in the CV. Hence, both peaks in the CV are attributed to CoTCPP reduction. The reduction potentials and assignments are summarized in Table 1.

The question then becomes at what potential are the trimeric cobalt clusters reduced? Unfortunately, spectral changes due to cluster reduction are not observed in the spectroelectrochemical experiments. This is not surprising due to the large discrepancy between the two molecular component's extinction coefficients.[27] However, the CV does have a large background current beginning at −900 mV that could be attributed to a molecular species. Similar molecular cobalt clusters have been

**Table 1. Reduction Potentials (vs ferrocyanide) for CoPIZA/FTO**

| reaction | $E_{1/2}$ | $E_p$ |
|---|---|---|
| (Co$^{III/II}$TCPP)CoPIZA | −1.04 V[a] | |
| Co$^{III/II}$cluster | ∼ −0.87 V[c] | |
| (Co$^{II/I}$TCPP)CoPIZA | −1.39 V[b] | −1.45 V[a] |
| Co$^{II/I}$cluster | ∼ −1.57 V[c] | |

[a]From CV. [b]From spectroelectrochemistry. [c]From ref 77.

investigated, and the Co$^{III}$ clusters display a reduction potential of −0.87 V vs ferrocyanide.[77] The Co$^{II/I}$ cluster reduction was found to occur at a potential of −1.57 V vs ferrocyanide.[77] Therefore, it is likely that the observed background current is due in part to the reduction of the nodal cobalt clusters. More interestingly, the nodal clusters of the CoPIZA have very similar reduction potentials to the CoTCPP struts. Therefore, it is possible that the redox hopping chain may involve CoTCPP−cobalt cluster exchange interactions. Replacement of the cobalt clusters with more insulating nodes, such as Zn or Zr, would provide support for cobalt cluster interaction and is an area of ongoing investigation. Overall, if the clusters are involved and the distance between redox centers is small, this would have a dramatic effect on the efficiency of charge transport.

There are two components to efficiency that can be addressed by the data collected: rate and potential. For applications in electrocatalysis, both parameters are extremely important. If the rate of charge transfer through the film is slow, this can be the overall rate-determining step to reactivity. It is highly undesirable to have a process not directly involved with catalytic transformation to be rate determining. Given that redox hopping is regarded as a diffusion process, the rate of charge transport is represented by the apparent diffusion coefficient ($D_{\text{app}}$) for charge transfer through the film. The apparent diffusion coefficient was determined from a fitting of the time-dependent spectroelectrochemical data by a modified Cottrell equation (eq 6).

$$\Delta A = \frac{2A_{\text{max}}D_{\text{app}}^{1/2}t^{1/2}}{d\pi^{1/2}} \qquad (6)$$

For CoPIZA/FTO, the $D_{\text{app}}$ is 7.55 (±0.05) × 10$^{-14}$ cm$^2$/s (Figure S7). The $D_{\text{app}}$ for charge transport between redox centers incorporated into polymer films range from 1 × 10$^{-11}$ to 1 × 10$^{-8}$ cm$^2$/s.[65,66,78,79] However, these coefficients may contain a component due to redox center displacement, where charge is transferred through the physical displacement and diffusion of the molecular components through the polymeric structure.[65,66,78,79] The theoretical analysis of diffusional transport in a single microcrystal performed by Scholz et al. found diffusion coefficients on the order 10$^{-8}$−10$^{-9}$ cm$^2$/s.[74−76] Given that diffusion in the CoPIZA/FTO system occurs in the absence of redox center displacement and across MOF grain boundaries as well as within individual MOF particles, the observed $D_{\text{app}}$ is reasonable for a redox hopping mechanism.

The diffusion of charge through CoPIZA/FTO is ambipolar in nature, with charge balancing anions/cations coupled to electron transport.[62,65,66,68,74] When CoPIZA is in the (Co$^{III}$TCPP)CoPIZA oxidation state, the film requires anions to balance the excess positive charge on the Co$^{III}$TCPP unit. Upon reduction to the neutral (Co$^{II}$TCPP)CoPIZA state, anion flow from the MOF is expected, eq 7.

$$e^- + [(Co^{III}TCPP)CoPIZA]\cdot ClO_{4(s)}$$
$$\rightarrow [(Co^{II}TCPP)CoPIZA]_{(s)} + ClO^-_{4(soln)} \qquad (7)$$
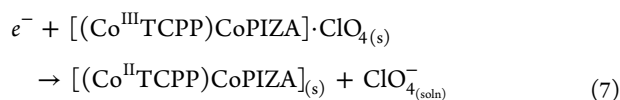
Further reduction of $(Co^{II}TCPP)CoPIZA$ to $[(Co^{II}TCPP)\text{-}CoPIZA]^-$ results in an overall negatively charged MOF backbone, eq 8. Therefore, cations are required to balance this excess charge.

$$Li^+_{(soln)} + [(Co^{II}TCPP)CoPIZA]_{(s)} + e^-$$
$$\rightarrow [(Co^{I}TCPP)CoPIZA]\cdot Li_{(s)} \qquad (8)$$
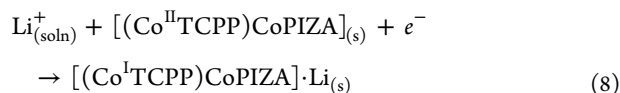
Electrochemical and spectroelectrochemical measurements do not allow for the individual components of the apparent diffusion coefficient, electron diffusion, and cation/anion diffusion to be distinguished; however, it is assumed that cation/anion diffusion is slower and, therefore, rate determining.[63]

Potential efficiency, defined here as potential required for an order of magnitude change in the ratio of reduced to oxidized film species, determines a component of overpotential. Overpotential is the potential difference between the thermodynamic potential of a reaction and the actual potential required to overcome kinetic barriers and drive the electrochemical process. The most efficient catalytic processes are driven at the thermodynamic limit. The potential efficiency for CoPIZA/FTO reduction was quantified from the nonideality factor in the Nernst equation fit to the spectroelectrochemical data (Figure 6, bottom inset). For accurate modeling, a nonideality factor of 2 was included. This means an order of magnitude change in concentration from oxidized film to reduced film required twice the amount of applied potential in comparison to a perfectly Nernstian process (59 vs 118 mV). Therefore, in the absence of overpotential for the catalysis itself, there is a built in overpotential of 59 mV from film reduction. Overall, this is relatively small, and very few electrochemical couples behave Nernstianly.[80,81] We attribute this overpotential to the insulating nature of the carboxylate links, which causes an ohmic drop over the thickness of the film. Hence, the molecular units far away from the CoPIZA/FTO interface "feel" a less negative potential than that applied to the FTO and, ultimately, require a more negative applied potential to be reduced.

For ultimate applications in electrocatalysis, balancing efficiency is stability. The stability of metal organic frameworks to oxidation state change is quite contentious.[7] Upon oxidation and reduction of any inorganic complex, it is likely that bond lengths and angles will change. For the most extreme cases, complete changes in coordination environment can occur. The most well-known example of this is a Jahn–Teller distortion.[82] However, CoPIZA exhibited surprising stability over the time course of both cyclic voltammetric and spectroelectrochemical experiments. The films could be cycled multiple times (>25) without a loss in peak current. Also, the maintenance of sharp isosbestic points in the spectroelectrochemical experiments indicates that the film was stable to both degradation and desorption, both of which would cause the isosbestic points to drift to lower absorbance values as the concentration of bound CoTCPP changed.

To investigate long-term stability, controlled potential electrolysis was performed on CoPIZA/FTO. A potential of −1.04 V vs ferrocene, corresponding to the $(Co^{III/II}TCPP)\text{-}CoPIZA$ reduction potential and beyond the expected $Co^{III/II}$

cluster reduction potential, was applied to the CoPIZA/FTO for 24 hs, after which time CoPIZA/FTO was characterized to determine whether structural degradation occurred. The SEM image showed no significant deterioration of the MOF film upon electrolysis (Figure S8). Additionally, no absorption features due to CoTCPP in solution were observed post-electrolysis. This indicates that the CoPIZA/FTO is stable to both $Co^{III/II}TCPP$ and, surprisingly, $Co^{III/II}$ cluster reduction. The same was repeated for the potential corresponding to the $(Co^{II/I}TCPP)CoPIZA$ reduction potential (−1.45 V vs ferrocyanide), after which time the film appears to be pitted (Figure S9), and absorption features due to dissolved CoTCPP were apparent in the spectrum of the solution postelectrolysis. While CoPIZA/FTO appears stable to $(Co^{II/I}TCPP)CoPIZA$ reduction over the time course of the spectroelectrochemical measurements, upon prolonged electrolysis the film degrades. The applied potential is on the edge of the expected $(Co^{II/I}cluster)CoPIZA$ reduction potential.[77] Therefore, reduction of the nodes would be inefficient and slow at this voltage. It follows that the observed CoPIZA/FTO degradation with prolonged electrolysis is most likely due to reduction of the framework nodes, breakdown of the cluster, and release of CoTCPP.

In light of this instability, pophyrinic films provide the ideal scaffold for determination of active catalytic species. As demonstrated, spectroscopic measurements can be used to monitor oxidation state changes upon the reduction of a substrate. This is an advantage over previous electrocatalytic MOF studies, which were limited to conclusions drawn from voltammetric response alone. To investigate the catalytic ability of the MOF film, the reduction of carbon tetrachloride by $(Co^{I}TCPP)CoPIZA$ was utilized. Metalloporphyrin organohalide reduction is well-known and used as a proof-of-concept example.[83,84] In the presence of carbon tetrachloride, an increase in current in the CV of CoPIZA/FTO at a potential commensurate with $(Co^{II/I}TCPP)CoPIZA$ reduction was observed (Figure 7A). Such an increase in current is indicative
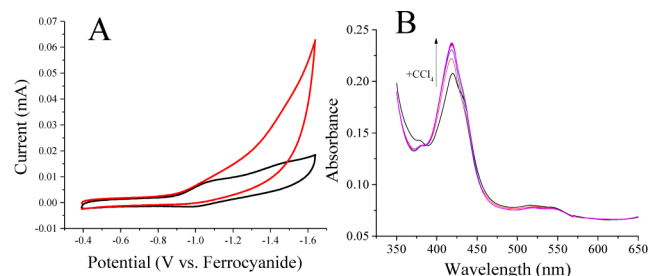
**Figure 7.** (A) Cyclic voltammetry of CoPIZA/FTO in 0.1 M LiClO$_4$/DMF (black) in the presence of CCl$_4$ (red) at 100 mV/s. (B) UV−vis spectra of the $(Co^{I}TCPP)CoPIZA$ and its oxidation to $(Co^{II}TCPP)\text{-}CoPIZA$ with the addition of CCl$_4$.

of catalytic activity of $(Co^{I}TCPP)CoPIZA$ toward CCl$_4$ reduction. To unequivocally assign the active catalytic state to $(Co^{I}TCPP)CoPIZA$, the spectral changes of the film were monitored during reactivity. After reduction to $(Co^{I}TCPP)\text{-}CoPIZA$ and injection of CCl$_4$, spectral features consistent with $(Co^{II}TCPP)CoPIZA$ were recovered (Figure 7B). Therefore, the observed catalysis was indeed due to intact MOF and neither deposition of a metal or metal oxide at the electrode surface nor free linker in solution.

## CONCLUSION

In summary, a new metalloporphyrin MOF thin film, CoPIZA/FTO, was prepared solvothermally, and the spectroscopic and electrochemical properties characterized. The open nature of the CoPIZA MOF network affords unrestricted access to the relatively large pores and unoccupied metal sites. Even with the moderate electrical conductivity exhibited by the CoPIZA/FTO, upon applied potential, the entire film could be reduced and remained stable for hours. The mechanism of charge transport was determined to be one of redox hopping, supported by both electrochemical and spectroelectrochemical analysis. The efficiency of reduction via redox hopping was found to be moderate with a rate consistent redox hopping mechanism and a slight overvoltage due to the potential drop across the film. The catalytic activity of CoPIZA/FTO was successfully demonstrated via the electrocatalytic reduction of $CCl_4$. This work provides a vital framework for further development of MOF thin films and their applications as electrocatalysts for a variety of reactions.

## EXPERIMENTAL SECTION

**Materials.** The following reagents and solvents were purchased from the indicated commercial suppliers: cobalt(II) chloride hexahydrate (Fluka Analytical); meso-tetra-(4-carboxy)tetraphenyl porphine (TCPP; Frontier Scientific); pyridine, ACS, 99.0% min, distilled before use (Alfa Aesar); potassium hydroxide (Sigma Aldrich); N,N-dimethylformamide (DMF), spectrophotometric grade (Spectrum); lithium perchlorate (Sigma Aldrich); fluorine-doped tin oxide (FTO; Hartford Glass).

**CoPIZA Thin Film Synthesis.** The thin film synthesis was developed based on the previously reported CoPIZA MOF synthesis.[31] To prepare a SAM of porphyrin, the FTO was first soaked in a pH 10 aqueous solution for 20 min. The FTO was then immersed in a TCPP/DMSO (0.1 mM) solution overnight. A mixture of $CoCl_2 \cdot 6H_2O$ (0.15 mmol) and TCPP (0.05 mmol) in 3.0 mL of 0.1 M pyridine/KOH was sonicated to mix. The mixture was then combined with the SAM-coated FTO in a sealed tube and heated at 150 °C for 2 days. The resulting purple powder was filtered, and the powder and thin film was washed with DMF.

**X-ray Photoelectron Spectroscopy (XPS).** XPS was conducted using a PHI 5300 spectrometer with a Perkin-Elmer Dual Anode X-ray source operating with magnesium radiation with monochromatic Mg Kα radiation (hν 1253.6 eV) at 13 kV and 250 W and a pass energy of 17.9 eV. A step size of 0.025 eV was used, and 180 sweeps were averaged. Emitted photoelectrons were detected by a hemispherical analyzer and the operating pressure in the sampling chamber was below $1 \times 10^{-7}$ Torr. The spectral scanning range for nitrogen 1s was 410−390 eV and for cobalt 2p was 765−815 eV. The spectra were calibrated according to the C 1s peak, which is known to occur at 284.6 eV.[85]

**Powder X-ray Diffraction (PXRD).** PXRD experiments were carried out on a Rigaku Altima IV with Cu(Kα) radiation (Cu-Kα = 0.15418 nm). A grazing incidence angle diffraction was used with a thin film stage. The PXRD measurements were carried out over a $2\theta$ range of 5−50° in continuous scanning mode with 0.05° steps at a rate of 0.5°/min.

**Microscopy Imaging.** *Scanning electron microscopy (SEM).* A LEO (Zeiss) 1550 field-emission scanning electron microscope at 5.0 kV was used for high-resolution images of the thin films.

*Atomic Force Microscopy (AFM).* A Veeco MultiMode AFM was operated in tapping mode to obtain the topology of the thin films.

**Attenuated Total Reflectance Fourier-Transform Infrared Spectroscopy (ATR-FTIR).** ATR-FTIR spectra were obtained on a Varian 670 FT-IR Spectrometer equipped with a diamond Specac Golden Gate attachment. All spectra are an average of 24 scans for powder samples and 6000 scans for thin films and were recorded from 4000 to 400 $cm^{-1}$ with 4 $cm^{-1}$ resolution. A background spectrum collected on air was subtracted from sample spectra. The spectra were not corrected for the depth of wavelength penetration.

**Steady-State UV−vis Absorption Spectroscopy.** Steady-state UV−vis absorption spectroscopy was performed on a Cary Series UV−vis NIR spectrophotometer. The wavelength was scanned from 800 to 200 nm with a data interval of 1.00 nm and scan rate of 600 nm/min.

**Electrochemical Impedance Spectroscopy (EIS).** EIS was performed with a Solartron SI 1260 Impedance analyzer controlled with a PC interface and Zplot 2.9 software. The sample was positioned between two gold-plated stainless steel electrodes to measure through-plane conductivity using a Solartron 12960 sample holder with a built-in micrometer and a frequency range from 3.2 MHz to 100 Hz. The AC amplitude applied was 10 mV with a frequency range from 16 mHz to 0.1 Hz. The film conductivity was obtained using the high-frequency intercept of the obtained Nyquist plot.

**Electrochemistry.** A BASi Epsilon potentiostat was employed for measurements in a three-electrode electrochemical cell with CoPIZA on FTO as the working electrode, platinum mesh as counter electrode, and Ag/AgCl (saturated KCl, aqueous) as reference in 0.1 M $LiClO_4$/DMF electrolyte. The Ag/AgCl was calibrated against the $Fe(CN)_6^{3-}$/$Fe(CN)_6^{4-}$ couple, where the expected $E_{1/2}$ is +361 mV vs NHE and Ag/AgCl is +197 mV vs NHE. The scan rate was varied over the range 10−1000 mV/s.

**Spectroelectrochemistry.** Spectroelectrochemistry was performed in a three-electrode arrangement containing the CoPIZA/FTO as working electrode, platinum mesh counter electrode, and Ag/AgCl (saturated KCl, aqueous) as reference. The electrochemical cell was set up in a quartz cuvette with a 24/40 joint capped with a rubber septum. The electrodes were immersed in a 0.1 M $LiClO_4$/DMF electrolyte solution and purged with nitrogen for 1 h. The potential was applied with a BASi Epsilon potentiostat, while the spectra were observed with a Cary Series UV−vis NIR spectrophotometer.

## ASSOCIATED CONTENT

**ⓢ Supporting Information**

PXRD data, AFM and SEM images, electrochemical data, standard UV−vis spectra, potential step spectroelectrochemistry, and conductivity data for CoPIZA on FTO. This material is available free of charge via the Internet at http://pubs.acs.org.

## AUTHOR INFORMATION

**Corresponding Author**
ajmorris@vt.edu

**Notes**
The authors declare no competing financial interest.

## ACKNOWLEDGMENTS

## REFERENCES

(1) Eddaoudi, M.; Kim, J.; Rosi, N.; Vodak, D.; Wachter, J.; O'Keeffe, M.; Yaghi, O. M. *Science* **2002**, *295*, 469.

(2) Rosi, N. L.; Eckert, J.; Eddaoudi, M.; Vodak, D. T.; Kim, J.; O'Keeffe, M.; Yaghi, O. M. *Science* **2003**, *300*, 1127.

(3) Caskey, S. R.; Wong-Foy, A. G.; Matzger, A. J. *J. Am. Chem. Soc.* **2008**, *130*, 10870.

(4) Sumida, K.; Rogow, D. L.; Mason, J. A.; McDonald, T. M.; Bloch, E. D.; Herm, Z. R.; Bae, T.-H.; Long, J. R. *Chem. Rev.* **2012**, *112*, 724.

(5) Ferey, G. *Chem. Soc. Rev.* **2008**, *37*, 191.

(6) Huxford, R. C.; Della, R. J.; Lin, W.-B. *Curr. Opin. Chem. Biol.* **2010**, *14*, 262.

(7) Lee, J. Y.; Farha, O. K.; Roberts, J.; Scheidt, K. A.; Nguyen, S. B. T.; Hupp, J. T. *Chem. Soc. Rev.* **2009**, *38*, 1450.

(8) Choi, J. H.; Choi, Y. J.; Lee, J. W.; Shin, W. H.; Kang, J. K. *Phys. Chem. Chem. Phys.* **2009**, *11*, 628.

(9) Ma, L.; Abney, C.; Lin, W. *Chem. Soc. Rev.* **2009**, *38*, 1248.

(10) Givaja, G.; Amo-Ochoa, P.; Gomez-Garcia, C. J.; Zamora, F. *Chem. Soc. Rev.* **2012**, *41*, 115.

(11) Khajavi, H.; Gascon, J.; Schins, J. M.; Siebbeles, L. D. A.; Kapteijn, F. *J. Phys. Chem. C* **2011**, *115*, 12487.

(12) Kuc, A.; Enyashin, A.; Seifert, G. *J. Phys. Chem. B* **2007**, *111*, 8179.

(13) Yang, L.-M.; Ravindran, P.; Vajeeston, P.; Tilset, M. *Phys. Chem. Chem. Phys.* **2012**, *14*, 4713.

(14) Pickup, P. G.; Murray, R. W. *J. Am. Chem. Soc.* **1983**, *105*, 4510.

(15) Wang, C.; Xie, Z.; de, K. K. E.; Lin, W. *J. Am. Chem. Soc.* **2011**, *133*, 13445.

(16) Narayan, T. C.; Miyakai, T.; Seki, S.; Dinca, M. *J. Am. Chem. Soc.* **2012**, *134*, 12932.

(17) Usov, P. M.; Fabian, C.; D'Alessandro, D. M. *Chem. Commun. (Cambridge, U. K.)* **2012**, *48*, 3945.

(18) Babu, K. F.; Kulandainathan, M. A.; Katsounaros, I.; Rassaei, L.; Burrows, A. D.; Raithby, P. R.; Marken, F. *Electrochem. Commun.* **2010**, *12*, 632.

(19) Hinogami, R.; Yotsuhashi, S.; Deguchi, M.; Zenitani, Y.; Hashiba, H.; Yamada, Y. *ECS Electrochem. Lett.* **2012**, *1*, H17.

(20) Senthil, K. R.; Senthil, K. S.; Anbu, K. M. *Electrochem. Commun.* **2012**, *25*, 70.

(21) Domenech, A.; Garcia, H.; Domenech-Carbo, M. T.; Llabres-i-Xamena, F. *Electrochem. Commun.* **2006**, *8*, 1830.

(22) Domenech, A.; Garcia, H.; Domenech-Carbo, M. T.; Llabres-i-Xamena, F. *J. Phys. Chem. C* **2007**, *111*, 13701.

(23) Lexa, D.; Saveant, J. M.; Soufflet, J. P. *J. Electroanal. Chem. Interfacial Electrochem.* **1979**, *100*, 159.

(24) Grinstaff, M. W.; Hill, M. G.; Labinger, J. A.; Gray, H. B. *Science* **1994**, *264*, 1311.

(25) Bhugun, I.; Lexa, D.; Saveant, J.-M. *J. Am. Chem. Soc.* **1996**, *118*, 1769.

(26) Chang, C. J.; Loh, Z.-H.; Shi, C.; Anson, F. C.; Nocera, D. G. *J. Am. Chem. Soc.* **2004**, *126*, 10013.

(27) Kadish, K.; Guilard, R., Smith, K. *The Porphyrin Handbook*; Academic Press: Waltham, MA, 2003.

(28) Suslick, K. S.; Bhyrappa, P.; Chou, J. H.; Kosal, M. E.; Nakagaki, S.; Smithenry, D. W.; Wilson, S. R. *Acc. Chem. Res.* **2005**, *38*, 283.

(29) Farha, O. K.; Shultz, A. M.; Sarjeant, A. A.; Nguyen, S. T.; Hupp, J. T. *J. Am. Chem. Soc.* **2011**, *133*, 5652.

(30) Meng, L.; Cheng, Q.; Kim, C.; Gao, W.-Y.; Wojtas, L.; Chen, Y.-S.; Zaworotko, M. J.; Zhang, X. P.; Ma, S. *Angew. Chem., Int. Ed.* **2012**, *51*, 10082.

(31) Kosal, M. E.; Chou, J.-H.; Wilson, S. R.; Suslick, K. S. *Nat. Mater.* **2002**, *1*, 118.

(32) Kosal, M. E.; Suslick, K. S. *J. Solid State Chem.* **2000**, *152*, 87.

(33) Fateeva, A.; Chater, P. A.; Ireland, C. P.; Tahir, A. A.; Khimyak, Y. Z.; Wiper, P. V.; Darwent, J. R.; Rosseinsky, M. J. *Angew. Chem., Int. Ed.* **2012**, *51*, 7440.

(34) Chen, Y.; Hoang, T.; Ma, S. *Inorg. Chem.* **2012**, *51*, 12600.

(35) Burnett, B. J.; Barron, P. M.; Choe, W. *CrystEngComm* **2012**, *14*, 3839.

(36) Son, H.-J.; Jin, S.; Patwardhan, S.; Wezenberg, S. J.; Jeong, N. C.; So, M.; Wilmer, C. E.; Sarjeant, A. A.; Schatz, G. C.; Snurr, R. Q.; Farha, O. K.; Wiederrecht, G. P.; Hupp, J. T. *J. Am. Chem. Soc.* **2013**, *135*, 862.

(37) Betard, A.; Fischer, R. A. *Chem. Rev. (Washington, DC, U. S.)* **2012**, *112*, 1055.

(38) Zacher, D.; Shekhah, O.; Woell, C.; Fischer, R. A. *Chem. Soc. Rev.* **2009**, *38*, 1418.

(39) Hermes, S.; Schroeder, F.; Chelmowski, R.; Woell, C.; Fischer, R. A. *J. Am. Chem. Soc.* **2005**, *127*, 13744.

(40) Shekhah, O.; Wang, H.; Kowarik, S.; Schreiber, F.; Paulus, M.; Tolan, M.; Sternemann, C.; Evers, F.; Zacher, D.; Fischer, R. A.; Woell, C. *J. Am. Chem. Soc.* **2007**, *129*, 15118.

(41) Shekhah, O.; Wang, H.; Strunskus, T.; Cyganik, P.; Zacher, D.; Fischer, R.; Woell, C. *Langmuir* **2007**, *23*, 7440.

(42) Li, W.-J.; Gao, S.-Y.; Liu, T.-F.; Han, L.-W.; Lin, Z.-J.; Cao, R. *Langmuir* **2013**, *29*, 8657.

(43) Stavila, V.; Volponi, J.; Katzenmeyer, A. M.; Dixon, M. C.; Allendorf, M. D. *Chem. Sci.* **2012**, *3*, 1531.

(44) So, M. C.; Jin, S.; Son, H.-J.; Wiederrecht, G. P.; Farha, O. K.; Hupp, J. T. *J. Am. Chem. Soc.* **2013**, *135*, 15698.

(45) Makiura, R.; Motoyama, S.; Umemura, Y.; Yamanaka, H.; Sakata, O.; Kitagawa, H. *Nat. Mater.* **2010**, *9*, 565.

(46) Xu, G.; Yamada, T.; Otsubo, K.; Sakaida, S.; Kitagawa, H. *J. Am. Chem. Soc.* **2012**, *134*, 16524.

(47) Motoyama, S.; Makiura, R.; Sakata, O.; Kitagawa, H. *J. Am. Chem. Soc.* **2011**, *133*, 5640.

(48) Burchill, P.; Welch, L. S. *Fuel* **1989**, *68*, 100.

(49) Glusker, J. P.; Trueblood, K. N. *Crystal Structura Analysis: A Primer*, 3rd ed.; Oxford University Press, Inc.: New York, 2010.

(50) Gouterman, M. *J. Mol. Spectrosc.* **1961**, *6*, 138.

(51) Balch, A. L.; Noll, B. C.; Olmstead, M. M.; Phillips, S. L. *Inorg. Chem.* **1996**, *35*, 6495.

(52) Silva, C. G.; Corma, A.; Garcia, H. *J. Mater. Chem.* **2010**, *20*, 3141.

(53) Alvaro, M.; Carbonell, E.; Ferrer, B.; Llabres, i. X. F. X.; Garcia, H. *Chem.—Eur. J.* **2007**, *13*, 5106.

(54) Fabregat-Santiago, F.; Garcia-Belmonte, G.; Bisquert, J.; Zaban, A.; Salvador, P. *J. Phys. Chem. B* **2002**, *106*, 334.

(55) Fikus, A.; Rammelt, U.; Plieth, W. *Electrochim. Acta* **1999**, *44*, 2025.

(56) Hotta, S.; Rughooputh, S. D. D. V.; Heeger, A. J.; Wudl, F. *Macromolecules* **1987**, *20*, 212.

(57) Xia, B. Y.; Wang, B.; Wu, H. B.; Liu, Z.; Wang, X.; Lou, X. W. *J. Mater. Chem.* **2012**, *22*, 16499.

(58) Wang, M.; Guo, D.-J.; Li, H.-L. *J. Solid State Chem.* **2005**, *178*, 1996.

(59) Li, L.; Duan, L.; Xu, Y.; Gorlov, M.; Hagfeldt, A.; Sun, L. *Chem. Commun. (Cambridge, U. K.)* **2010**, *46*, 7307.

(60) Huang, S.-Y.; Ganesan, P.; Popov, B. N. *Appl. Catal. B* **2011**, *102*, 71.

(61) Bard, A. J. *Electroanalytical Chemistry*; Marcel Dekker, Inc.: New York, 1984; Vol. 13.

(62) Daum, P.; Lenhard, J. R.; Rolison, D.; Murray, R. W. *J. Am. Chem. Soc.* **1980**, *102*, 4649.

(63) Rudge, A.; Raistrick, I.; Gottesfeld, S.; Ferraris, J. P. *Electrochim. Acta* **1994**, *39*, 273.

(64) Chidsey, C. E. D.; Bertozzi, C. R.; Putvinski, T. M.; Mujsce, A. M. *J. Am. Chem. Soc.* **1990**, *112*, 4301.

(65) Martin, C. R.; Rubinstein, I.; Bard, A. J. *J. Am. Chem. Soc.* **1982**, *104*, 4817.

(66) Buttry, D. A.; Anson, F. C. *J. Electroanal. Chem. Interfacial Electrochem.* **1981**, *130*, 333.

(67) Yagi, M.; Mitsumoto, T.; Kaneko, M. *J. Electroanal. Chem.* **1997**, *437*, 219.

(68) Daum, P.; Murray, R. W. *J. Electroanal. Chem. Interfacial Electrochem.* **1979**, *103*, 289.

(69) Bard, A. J. F., L., R. *Electrochemical Methods: Fundamentals and Applications*, 2nd ed.; John Wiley & Sons, Inc.: New York, 2001.

(70) Kaufman, F. B.; Engler, E. M. *J. Am. Chem. Soc.* **1979**, *101*, 547.

(71) Kaufman, F. B.; Schroeder, A. H.; Engler, E. M.; Kramer, S. R.; Chambers, J. Q. *J. Am.* **1980**, *102*, 483.

(72) Schroeder, A. H.; Kaufman, F. B.; Patel, V.; Engler, E. M. *J. Electroanal. Chem. Interfacial Electrochem.* **1980**, *113*, 193.

(73) Yagi, M.; Sato, T. *J. Phys. Chem. B* **2003**, *107*, 4975.

(74) Lovric, M.; Scholz, F. *J. Solid State Electrochem.* **1997**, *1*, 108.

(75) Lovric, M.; Scholz, F. *J. Solid State Electrochem.* **1999**, *3*, 172.

(76) Schroder, U.; Oldham, K. B.; Myland, J. C.; Mahon, P. J.; Scholz, F. *J. Solid State Electrochem.* **2000**, *4*, 314.

(77) Beattie, J. K.; Beck, C. U.; Lay, P. A.; Masters, A. F. *Inorg. Chem.* **2003**, *42*, 8366.

(78) Yagi, M.; Sato, T. *J. Phys. Chem. B* **2003**, *107*, 4975.

(79) Yagi, M.; Mitsumoto, T.; Kaneko, M. *J. Electroanal.* **1997**, *437*, 219.

(80) Koval, C. A.; Anson, F. C. *Anal. Chem.* **1978**, *50*, 223.

(81) Kohl, P. A.; Bard, A. J. *J. Am. Chem. Soc.* **1977**, *99*, 7531.

(82) Longuet-Higgins, H. C.; Opik, U.; Pryce, M. L.; Sack, R. A. *Proc. R. Soc. London, Ser. A* **1958**, *244*, 1.

(83) Lexa, D.; Saveant, J. M.; Su, K. B.; Wang, D. L. *J. Am. Chem. Soc.* **1987**, *109*, 6464.

(84) Obare, S. O.; Ito, T.; Meyer, G. J. *Environ. Sci. Technol.* **2005**, *39*, 6266.

(85) Moulder, J. F.; Stickle, W. F.Sobol, P. E.; Bombem, K. D. *Handbook of X-ray Photoelectron Spectroscopy*; Physical Electronics, Inc.: Chanhassen, MN, 1995.